RSC Advances

PAPER

View Article Online
View Journal | View Issue

Cite this: *RSC Adv.*, 2014, **4**, 61

Low dimensional cyano-bridged heterobimetallic M–Fe^{III} (M = Ni^{II}, Cu^{II}) complexes constructed from *Mer*-$[Fe^{III}(qcq)(CN)_3]^-$ building blocks: syntheses, structures and magnetic properties†

Hongbo Zhou,[a] Jiahao Yan,[a] Xiaoping Shen,*[a] Hu Zhou[b] and Aihua Yuan[b]

Received 18th September 2013
Accepted 29th October 2013

DOI: 10.1039/c3ra45218b

www.rsc.org/advances

Four cyano-bridged heterobimetallic trinuclear complexes, $\{[Ni(en)_2][Fe(qcq)(CN)_3]_2\}\cdot 2H_2O$ (**1**) [en = 1,2-ethylenediamine; qcq^- = 8-(2-quinoline-2-carboxamido)quinoline anion], $\{[Ni(teta)][Fe(qcq)(CN)_3]_2\}\cdot 2DMF\cdot 2H_2O$ (**2**) (teta = 5,5,7,12,12,14-hexamethyl-1,4,8,11-tetraazacyclotetradecane, DMF = *N*,*N*-dimethylformamide), $\{[CuL^1][Fe(qcq)(CN)_3]_2\}\cdot 0.61H_2O$ (**3**) (L^1 = 3,10-dibutyl-1,3,5,8,10,12-hexaazacyclotetradecane) and $\{[CuL^2][Fe(qcq)(CN)_3]_2\}\cdot 4.75H_2O$ (**4**) (L^2 = 3,10-dipropyl-1,3,5,8,10,12-hexaazacyclotetradecane) have been synthesized and characterized both structurally and magnetically. The structural analyses reveal that **1–4** are all trinuclear centrosymmetric clusters, and the intercluster π–π interactions and hydrogen bonds extend **1–4** into high dimensional supermolecular networks. Magnetic investigation indicates that **1** and **2** exhibit intracluster ferromagnetic couplings accompanied by significant magnetic anisotropy. In contrast, **3** and **4** show unusual intracluster antiferromagnetic couplings, which could even be decoupled by a strong applied field.

Introduction

Single molecule magnets (SMM)[1] and single chain magnets (SCM),[2] which are called low-dimensional molecular magnets,[3] have been attracting much attention from chemists and physicists because of their potential applications in molecular devices, high-density information storage, quantum computing and so on.[4] To date, a great number of magnetic complexes have been investigated for the purpose of clarifying the magnetic mechanism so as to design ideal magnetic materials. Among various magnetic systems studied, coordination complexes especially the cyano-bridged magnetic assemblies are of special importance because the cyanide groups (CN^-) can mediate effectively the magnetic exchanges between the spin carriers and moreover, the linear coordination mode of cyanide groups makes the structure of target systems more predictable, facilitating the structure designs and the analyses of magneto–structural correlation.[5] Cyanometalates building blocks such as the hexacyanometalates $[M(CN)_6]^{q-}$ (M = Fe, Cr, Mn, or V) have provided a large family of three-dimensional complexes known as Prussian blue analogues, which exhibit extremely high critical temperature (T_c) even up to room temperature.[6] Recently, another synthetic strategy based on the modified hexacyanometalates of $[(L)M(CN)_p]^{q-}$ (where L = polydentate N/O-ligands; M = Cr, Fe, *etc.*) have been investigated by introducing various polydentate ligands of L into the cyanometalates.[7] Different from hexacyanometalates that are used for three-dimensional molecular magnets, the modified hexacyanometalates are designed for low dimensional systems that behave possibly as SMMs and SCMs, in which the selection of polydentate ligands L (also called capping ligands) are very important: (i) the tailored organic ligands make the self-assembly reaction more controllable, limit the oligomerization or polymerization effect and promote the formation of the low-dimensional structures. (ii) The molecular geometries of blocking group L define the molecular orbitals and affect greatly the magnetic coupling mechanism and anisotropy. (iii) The intermolecular magnetic interactions, which are also critical to low dimensional magnetism, can be readily tuned by varying the capping ligands. Especially, tricyanidoferrate of $[(L)Fe(CN)_3]^{3-}$ has aroused intense interest because of its flexible facial (*fac*-) and meridian (*mer*-) coordination modes depending on the capping ligand L.[8] The facially coordinate ligands such as hydrotris(pyrazol-1-yl)borate (Tp), hydrotris(3,5-dimethylpyrazol-1-yl) borate (Tp*), tetra(pyrazol-1-yl)borate (pzTp), and 1,3,5-triaminocyclohexane (tach) have been well investigated,[9] and some of the related complexes such as $[\{(pzTp)Fe(CN)_3\}_2\{Ni(bipy)_2\}]\cdot$

[a]*School of Chemistry and Chemical Engineering, Jiangsu University, Zhenjiang 212013, China. E-mail: xiaopingshen@163.com; Fax: +86-511-8879180; Tel: +86-511-88791800*

[b]*School of Material Science and Engineering, Jiangsu University of Science and Technology, Zhenjiang 212003, China*

† Electronic supplementary information (ESI) available: The intermolecular short contacts and packing diagrams of **1–4** in Fig. S1 and S2. CCDC 948658–948661. For ESI and crystallographic data in CIF or other electronic format see DOI: 10.1039/c3ra45218b

$2H_2O$[10] and $[\{(Tp^{*Bn})Fe(CN)_3\}_2\{Ni(DMF)_4\}]\cdot 2DMF$[9g] exhibit interesting SMM behaviors. However, relatively less attentions have been paid to *mer*-tricyanidoferrate (Scheme 1a) although several complexes derived from *mer*-$[Fe(L)(CN)_3]^-$ have been reported.[11–14] In this work, we focus our interest on a recently reported *mer*-tricyanidoferrate building block, $[Fe^{III}(qcq)(CN)_3]^-$[qcq^- = 8-(2-quinoline-2-carboxamido)quinoline anion],[15] from which four new cyano-bridged heterobimetallic trinuclear complexes, $\{[Ni(en)_2][Fe(qcq)(CN)_3]_2\}\cdot 2H_2O$ (**1**) [en = 1,2-ethylenediamine; qcq^- = 8-(2-quinoline-2-carboxamido)quinoline anion], $\{[Ni(teta)][Fe(qcq)(CN)_3]_2\}\cdot 2DMF\cdot 2H_2O$ (**2**) (teta = 5,5,7,12,12,14-hexamethyl-1,4,8,11-tetraazacyclotetradecane, DMF = *N*,*N*-dimethylformamide), $\{[CuL^1][Fe(qcq)(CN)_3]_2\}\cdot 0.61H_2O$ (**3**) (L^1 = 3,10-dibutyl-1,3,5,8,10,12-hexaazacyclotetradecane) and $\{[CuL^2][Fe(qcq)(CN)_3]_2\}\cdot 4.75H_2O$ (**4**) (L^2 = 3,10-dipropyl-1,3,5,8,10,12-hexaazacyclotetradecane) have been synthesized by a chemical self-assembly method (teta, L^1 and L^2 are shown in Scheme 1b). Herein, we report the syntheses, crystal structures and magnetic properties of the four complexes.

Experimental

Physical measurements

Elemental analyses for C, H and N were performed at a Perkin-Elmer 240C analyzer. Ni, Cu and Fe analyses were made on a Jarrell-Ash 1100 + 2000 inductively coupled plasma quantometer (ICP). IR spectra were recorded on a Nicolet FT-170SX spectrometer with KBr pellets in the 4000–400 cm^{-1} region. All magnetic measurements on microcrystalline samples were conducted on a Quantum Design MPMP-XL7 superconducting quantum interference device (SQUID) magnetometer. Corrections of measured susceptibilities were carried out considering both the sample holder as the background and the diamagnetism of the constituent atoms according to Pascal's tables.[16]

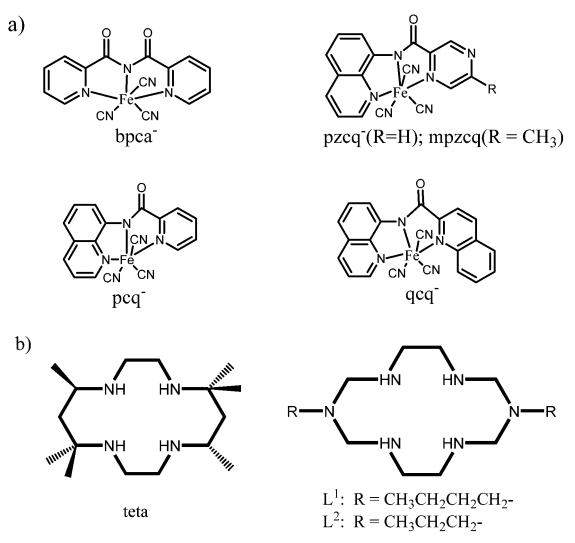

Scheme 1 (a) Typical *mer*-tricyanidoferrate building blocks; (b) macrocyclic ligands of teta, L^1 and L^2.

Caution! *Cyanides are highly toxic and perchlorate salts of metal complexes are potentially explosive. So handing them carefully with small quantities is highly suggested for the safety consideration.*

Syntheses

Starting materials. All chemicals and solvents were reagent grade and were used without further purification. $PPh_4[Fe(qcq)(CN)_3]$,[15] $[Ni(en)_2](ClO_4)_2$, $[Ni(teta)](ClO_4)_2$,[17] $[CuL^1](ClO_4)_2$ and $[CuL^2](ClO_4)_2$ (ref. 18) were prepared according to the literature methods.

$\{[Ni(en)_2][Fe(qcq)(CN)_3]_2\}\cdot 2H_2O$ (1). **1** was obtained as block black crystals by slow diffusion of a methanol solution (10 mL) of $PPh_4[Fe(qcq)(CN)_3]$ (0.1 mmol) and an aqueous solution (10 mL) of $[Ni(en)_2](ClO_4)_2$ (0.05 mmol) through a H-shaped tube at room temperature for about two weeks. The resulting crystals were collected, washed with H_2O and CH_3OH, and dried in air. Anal. found: C, 53.13; H, 4.27; N, 20.43; Fe, 10.56; Ni, 5.25%. Calcd for $C_{48}H_{44}Fe_2NiN_{16}O_4$: C, 53.41; H, 4.11; N, 20.76; Fe, 10.35; Ni, 5.44%. IR: ν_{max}/cm^{-1} 3416(s), 2119(m), 1648(s), 1504(m), 1459(m), 1436(m), 1384(m), 1342(m), 1214(w), 1151(m), 1020(m), 773(m).

$\{[Ni(teta)][Fe(qcq)(CN)_3]_2\}\cdot 2DMF\cdot 2H_2O$ (2). **2** was also obtained as block black crystals by slow diffusion of a methanol solution (10 mL) of $PPh_4[Fe(qcq)(CN)_3]$ (0.1 mmol) and a water–DMF (v/v = 1 : 4) solution (10 mL) of $[Ni(teta)](ClO_4)_2$ (0.05 mmol) through a H-shaped tube at room temperature for about two weeks. The resulting crystals were collected, washed with H_2O and CH_3OH, and dried in air. Anal. found: C, 56.86; H, 5.81; N, 17. 99; Fe, 8.11; Ni, 4.23%. Calcd for $C_{66}H_{78}Fe_2NiN_{18}O_6$: C, 57.04; H, 5.66; N, 18.14; Fe, 8.04; Ni, 4.22%. IR: ν_{max}/cm^{-1} 3435(s), 2119(m), 1633(s), 1504(w), 1461(m), 1436(s), 1388(m), 1342(m), 1214(w), 1155(m), 1097(s), 725(m).

$\{[CuL^1][Fe(qcq)(CN)_3]_2\}\cdot 0.61H_2O$ (3). **3** was obtained as deep red crystals by slow diffusion of a methanol solution (10 mL) of $PPh_4[Fe(qcq)(CN)_3]$ (0.1 mmol) and a DMF solution (10 mL) of $[CuL^1](ClO_4)_2$ (0.05 mmol) through a H-shaped tube at room temperature for about several weeks. The resulting crystals were collected, washed with DMF and CH_3OH, and dried in air. Anal. found: C, 56.23; H, 5.45; N, 19.28; Fe, 8.51; Cu, 4.88%. Calcd for $C_{60}H_{63.22}CuFe_2N_{18}O_{2.61}$: C, 57.49; H, 5.08; N, 20.11; Fe, 8.91; Cu, 5.07%. IR: ν_{max}/cm^{-1} 3423(s), 3233(m), 2112(m), 1633(s), 1504(m), 1463(m), 1386(s), 1344(m), 1213(w), 1153(m), 1014(m), 767(m).

$\{[CuL^2][Fe(qcq)(CN)_3]_2\}\cdot 4.75H_2O$ (4). Similar to **3**, **4** was also obtained as deep red crystals by slow diffusion of a methanol solution (10 mL) of $PPh_4[Fe(qcq)(CN)_3]$ (0.1 mmol) and a DMF solution (10 mL) of $[CuL^2](ClO_4)_2$ (0.05 mmol) through a H-shaped tube at room temperature for about several weeks. The resulting crystals were collected, washed with DMF and CH_3OH, and dried in air. Anal. found: C, 52.53; H, 5.25; N, 19.28; Fe, 8.37; Cu, 4.68%. Calcd for $C_{58}H_{67.5}CuFe_2N_{18}O_{6.75}$: C, 53.59; H, 5.23; N, 19.39; Fe, 8.59; Cu, 4.89%. IR: ν_{max}/cm^{-1} 3432(s), 3233(m), 2111(m), 1627(s), 1504(m), 1463(m), 1386(s), 1344(m), 1213(w), 1153(m), 1014(m), 767(m).

Table 1 Details of the crystallographic data collection, structural determination and refinement for **1–4**

	1	**2**	**3**	**4**
Formula	$C_{48}H_{44}Fe_2NiN_{16}O_4$	$C_{66}H_{78}Fe_2NiN_{18}O_6$	$C_{60}H_{63.22}CuFe_2N_{18}O_{2.61}$	$C_{58}H_{67.5}CuFe_2N_{18}O_{6.75}$
F_W	1079.40	1389.87	1253.50	1300.01
Crystal system	Triclinic	Monoclinic	Triclinic	Triclinic
Space group	$P\bar{1}$	$C2/c$	$P\bar{1}$	$P\bar{1}$
a/Å	9.3769(16)	25.8501(15)	10.283(2)	10.350(2)
b/Å	10.441(2)	16.246(2)	12.391(3)	12.023(3)
c/Å	14.992(3)	19.5463(13)	13.032(3)	12.921(3)
α/°	90.311(2)	90.00	107.05(3)	101.583(3)
β/°	106.740(3)	121.075(4)	94.67(3)	94.969(3)
γ/°	104.011(2)	90.00	94.81(3)	94.440(3)
V/Å^3	1359.3(4)	7030.8(11)	1572.2(5)	1561.8(6)
Z	1	4	1	1
ρ_{calcd}/g cm^{-3}	1.319	1.313	1.323	1.372
$F(000)$	556	2912	649.8	667
θ/°	3.09–25.91	3.48–26.03	3.15–25.00	1.62–24.99
Index ranges	$-10 \le h \le 11$	$-31 \le h \le 31$	$-12 \le h \le 11$	$-11 \le h \le -12$
	$-12 \le k \le 12$	$-19 \le k \le 20$	$-14 \le k \le 14$	$-13 \le k \le 14$
	$-18 \le l \le 16$	$-24 \le l \le 17$	$-15 \le l \le 14$	$-15 \le l \le 15$
Total/unique data	12 576/5140	16 527/6759	13 145/5466	11 219/5437
Observed data [$I > 2\sigma(I)$]	3169	5101	4611	3955
R_{int}	0.0519	0.0385	0.0412	0.0355
Data/restraints/parameters	3169/0/340	5101/0/435	4611/16/388	3955/29/390
GOF on F^2	1.054	1.033	1.016	1.069
$R_1[I > 2\sigma(I)]$	0.0607	0.0509	0.0750	0.0480
wR_2 (all data)	0.1297	0.1257	0.1601	0.1356

X-Ray structure determination

Diffraction data were collected on a Bruker *SMART APEX CCD* area detector diffractometer using graphite-monochromated Mo-K$_\alpha$ radiation (λ = 0.71073 Å) with the φ and ω scan mode. Diffraction data analysis and reduction were performed with *SMART*, *SAINT* and *XPREP*.[19] Absorption corrections were performed with *SADABS*.[20] Structures were solved using direct method and refined by full-matrix least-squares techniques based on F^2 using SHELXL-97.[21] All non-hydrogen atoms of **1–4** were refined with anisotropic thermal parameters. The H atoms of all chelated ligands and DMF molecules were calculated at idealized positions, but the water–H atoms in **1** and **2** are located from difference maps with all the H atoms refined in a riding mode. The water molecules in **1** and **2** were assigned with partial occupancy factor. For **3** and **4**, the water oxygen atoms (water–H atoms are not found) are not present with unit occupancy, and it is allowed a anisotropic free variable refinement with partial occupancy. The pendant groups of the macrocyclic ligands in **3** and **4** split into two different positions and a few distance or angle restraints (see refine special details in CIF file) were used in the refinement. The crystallographic data and experimental details for structural analyses are summarized in Table 1.

Results and discussion

Synthesis and characterization

In this paper, $[Fe(qcq)(CN)_3]^-$ was used as a building block to prepare the low-dimensional complexes. In fact, the solubility of A[Fe(qcq)(CN)$_3$] (A = counter cations) is highly dependent on the counter cation selected because different solvent polarity favors different type of cations. For instance, $PPh_4[Fe(qcq)(CN)_3]$ can be well dissolved in methanol but insoluble in water, while K[Fe(qcq)(CN)$_3$] is just on the contrary. In this study, $PPh_4[Fe(qcq)(CN)_3]$ is used instead of K[Fe(qcq)(CN)$_3$] because the latter is insoluble in methanol. To confirm this point, we also used K[Fe(qcq)(CN)$_3$] as the building block and unfortunately, no suitable crystals were obtained, indicating the subtle reaction mechanism and the important role of PPh_4^+ cation for the growth of the crystals. The reactions of $PPh_4[Fe(qcq)(CN)_3]$ with $[Ni(en)_2](ClO_4)_2$ or [Ni(teta)](ClO$_4$)$_2$ both gave block black crystals, which are stable in room temperature and show insolubility in water and methanol. By replacing the nickel complexes with copper precursors, deep red crystals were formed, which also exhibit high stabilities. With the same solubility consideration, DMF was used for the syntheses of **2**, **3** and **4** because the precursors of [Ni(teta)](ClO$_4$)$_2$, $[CuL^1](ClO_4)_2$ and $[CuL^2](ClO_4)_2$ are more soluble in DMF than in water. IR spectroscopy for **1–4** all displayed absorption peaks in 2100–2150 cm^{-1}, indicating the presence of cyanide groups in these complexes.[22] The similarity of the IR spectra of these complexes is obviously due to the comparable structural moieties presented in the molecular units.

Description of the structures

The key bond distances and angles for **1–4** are listed in Table 2. The molecular structural diagrams of **1–4** are shown in Fig. 1, and the intermolecular packing diagrams including the intermolecular short contacts are shown in Fig. S1 and S2 in ESI.†

Structures of complexes 1 and 2. Complexes **1** and **2** show similar structural styles and thus they are discussed together

Table 2 Selected bond lengths [Å] and angles [degree] for **1–4**

1		**2**		**3**		**4**	
C1–Fe1	1.962(4)	C20–Fe1	1.968(3)	C1–Fe1	1.959(5)	C1–Fe1	1.958(4)
C2–Fe1	1.957(5)	C21–Fe1	1.922(3)	C2–Fe1	1.959(6)	C2–Fe1	1.955(4)
C3–Fe1	1.971(5)	C22–Fe1	1.950(3)	C3–Fe1	1.952(6)	C3–Fe1	1.957(4)
Fe1–N5	1.922(3)	Fe1–N2	1.947(2)	Fe1–N5	1.888(2)	Fe1–N5	1.890(3)
Fe1–N6	2.010(3)	Fe1–N3	1.964(2)	Fe1–N6	1.977(2)	Fe1–N6	1.971(3)
Fe1–N4	2.018(3)	Fe1–N1	2.048(3)	Fe1–N4	2.009(2)	Fe1–N4	2.001(3)
N1–Ni1	2.137(3)	N6–Ni1	2.112(3)	Cu1–N8	2.001(4)	Cu1–N8	2.006(3)
N7–Ni1	2.085(3)	N7–Ni1	2.111(2)	Cu1–N7	2.005(2)	Cu1–N7	2.014(3)
N8–Ni1	2.126(4)	N8–Ni1	2.073(2)	Cu1–N1	2.568(2)	Cu1–N1	2.559 (2)
C1–N1–Ni1	161.5(3)	C22–N6–Ni1	165.2(2)	C1–N1–Cu1	142.2(2)	C1–N1–Cu1	143.1(2)
N1–C1–Fe1	175.8(4)	N4–C20–Fe1	175.2(3)	N1–C1–Fe1	173.6 (4)	N1–C1–Fe1	173.7(3)
N2–C2–Fe1	178.4(4)	N5–C21–Fe1	179.0(3)	N2–C2–Fe1	177.9(4)	N2–C2–Fe1	178.1(3)
N3–C3–Fe1	177.8(4)	N6–C22–Fe1	175.7(2)	N3–C3–Fe1	178.1 (4)	N3–C3–Fe1	177.0(3)

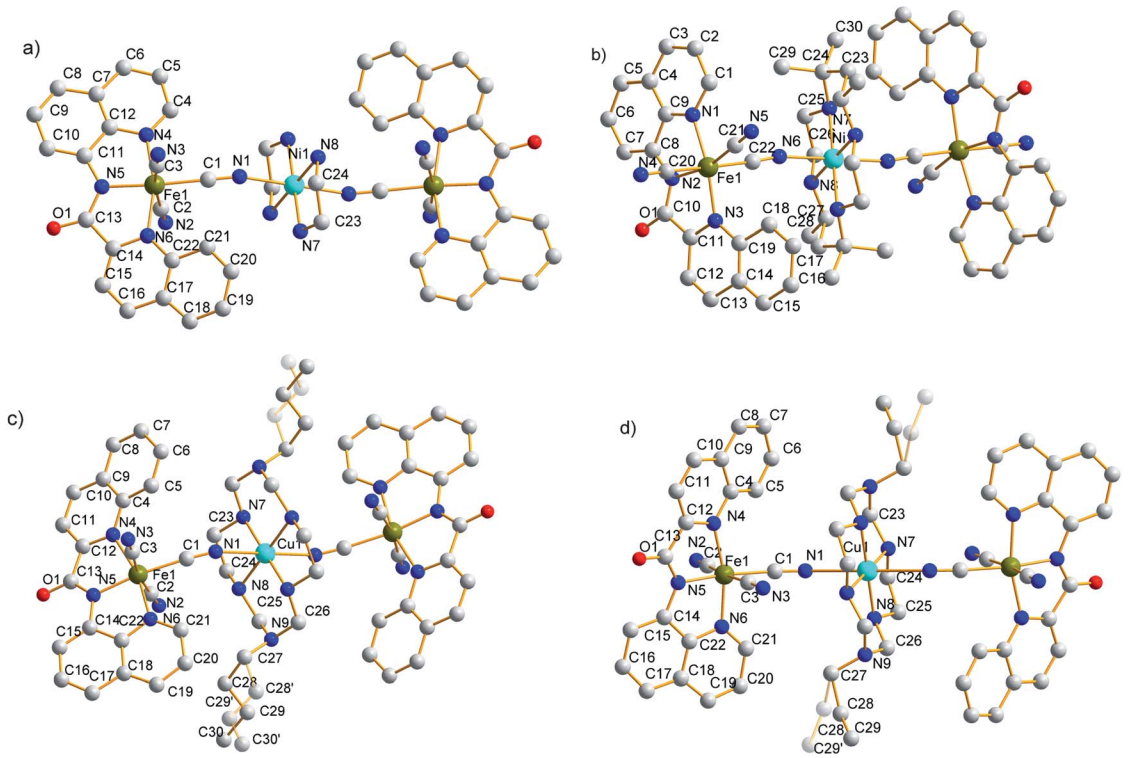

Fig. 1 Molecular structures with selected atom-labeling schemes for **1** (a), **2** (b), **3** (c) and **4** (d). (The solvents molecules are omitted for clarity).

although they crystallize in different space groups and have different chelating ligands coordinated to central Ni^{2+} ions. As shown in Fig. 1(a and b), the molecular units of **1** and **2** are neutral centrosymmetric trinuclear entities with Ni atom lying on the inversion centre. Within the cluster, the central $[Ni(L')]^{2+}$ (L′ = en, teta) unit is axially linked to two $[Fe(qcq)(CN)_3]^-$ anions *via* bridging cyanides in *trans*-mode, resulting in hexa-coordinated Ni with the equatorial sites occupied by two bidentate ligands of en or one tetradentate ligand of teta. The $Ni–N_{cyanide}$ bond distances for **1** (Ni1–N1) and **2** (Ni1–N6) are 2.137(3) and 2.112(3) Å, respectively, which is close to the values of the analogous complexes reported before.[9f,23–28] The $Ni–N_{amine}$ bond distances for **1** and **2** are 2.085(3)–2.126(4) Å and 2.073(2)–2.111(2) Å, respectively. The Ni–N≡C bond angles of **1** and **2** are 161.5(3) and 165.2(2)°, respectively, exhibiting obvious deviation from linearity. For the moieties of $[Fe(qcq)(CN)_3]^-$, the coordination environment of Fe center can be described as distorted octahedron, consisting of three C atoms from cyanide groups and three N atoms from qcq^-. The Fe–C bond lengths are nearly close to each other (1.922(3)–1.971(5) Å). However, Fe–N bond distances [1.922(3)–2.048(3) Å] deviate from each other with the smallest value found for the Fe–N (amide) bonds [1.922(3) Å (Fe1–N5) for **1**; 1.947(2) Å (Fe1–N2) for **2**]. The relatively shorter Fe–N (amide) bond distances than those for Fe–N

(aromatic rings) might be attributed to the strong σ-donor effect of the deprotonated amide.[15] Different from the bent Ni–N≡C bond angles, the Fe–C≡N bond angles for **1** and **2** are nearly linear (175.2(3)–179.0(3)°). It is worth noting that the two planes of quinoline rings (C4–C12 and C14–C22) from qcq^- in **1** are obviously noncoplanar with dihedral angle being as high as 27.6(2)°, which is significantly larger than that [3.2(5)°] found in **2**, possibly owing to the different coordinating modes of $[Fe(qcq)(CN)_3]^-$ in **1** and **2**. For **1**, the bridging cyanide (C1≡N1) is nearly coplanar with the quinoline rings leaving two terminal cyanides (C2≡N2, C2≡N2) in *trans*-mode, while that (C22≡N6) in **2** is basically perpendicular to the quinoline rings keeping the two terminal cyanides (C21≡N5, C20≡N4) in *cis*-mode. The former coordination fashion might produce larger steric effects than the latter one, and thus the quinoline rings planes in **1** are highly distorted.

Since **1** and **2** crystallize in different space groups (P-1 for **1**, C2c for **2**), different intermolecular packing structures are formed. As shown in Fig. S1a,† the trinuclear units of **1** interact with each other *via* π···π stacking (centroid to centroid distance: 4.2 Å) of adjacent quinoline rings along *c* axis, forming 1-D supramolecular chains, which then arrange in parallel with significant hydrogen bonds interactions (mediated *via* water–H and terminal cyanide nitrogen atoms with the maximum D–H···A distance shorter than 2.1 Å). The molecular units of **2** also interact with each other *via* π···π stacking of adjacent quinoline rings (centroid to centroid distance: 3.6–3.9 Å), but different from **1**, a 2-D grid-like supramolecular network is formed in *ab* plane, and the molecules of DMF are situated in the square holes (Fig. S1b†). Moreover, hydrogen bonds interactions mediated *via* solvent molecules are also observed in **2** though they seem to be rather weak (minimum D–H···A distance larger than 3.0 Å).

Structures of complexes 3 and 4. Complexes **3** and **4** show comparable structure to **1** and **2** though the $[Ni(L)]^{2+}$ moieties are replaced with $[Cu(L)]^{2+}$. As shown in Fig. 1(c and d), **3** and **4** also show linear centrosymmetric trinuclear cluster structure. In the molecules, central Cu ion is six-coordinated by N atoms with four N atoms from the macrocyclic ligands L defining the equatorial plane and two N atoms from two bridging cyanide groups occupying the axial positions, leading to an octahedron configuration. Different from **1** and **2**, significant Jahn–Teller effect is observed for **3** and **4**, which is evidenced by that the $Cu–N_{axial}$ bond lengths [2.568(2) Å for **3**; 2.559(2) Å for **4**] is much longer than the $Cu–N_{equatorial}$ bond distances [2.001(4)–2.005(2) Å for **3**; 2.006(3)–2.014(3) Å for **4**]. Comparable to other cyano-bridged Cu···Fe systems,[9f,23,29] the Cu–N≡C bonds are highly bent with the bond angles of 142.2(2)° for **3** and 143.1(2)° for **4**, respectively. For the macrocyclic ligands L, the pendant groups in **3** (C27, C28, C29, C30) and **4** (C27, C28, C29) are highly disordered and split into two different positions, which should be originated from the average of the crystallographic sites. For the $[Fe(qcq)(CN)_3]^-$ unit in **3** and **4**, all the Fe–C bond lengths are highly consistent [1.952(6)–1.959(6) Å for **3**, 1.955(4)–1.958(4) Å for **4**], while the Fe–N bond distances [1.888(2)–2.009(2) Å for **3** and 1.890(3)–2.001(3) Å for **4**] deviate from each other, which is comparable to that found in **1** and **2**. For the bond angles of Fe–C≡N in **3** and **4**, the terminal ones range from 177.0(3)° to 178.1(4)°, while bridging ones are more bent with the value of 173.6 (4)°–173.7(3). In addition, noncoplanar quinoline rings of qcq^- in **3** and **4** are also found with the dihedral angles of 24.7(5)° and 23.9(2)°, respectively, which is comparable to the case of **1**.

For packing structures (Fig. S2†), **3** and **4** feature the similar fashions. The clusters interact with each other *via* π···π stacking of adjacent quinoline rings [centroid to centroid distance: 3.8–4.4 Å (**3**) and 3.7–4.0 Å (**4**)], affording 2-D supramolecular layered networks. Each layer is well separated with average separations of 8.3 Å for **3** and 7.0 Å for **4**, respectively. Hydrogen bonds interactions should also widely exist in **3** and **4** although it is not possible to analysis in detail due to the disorder of solvents molecules.

Magnetic properties

Magnetic properties of 1 and 2. The temperature dependent susceptibilities under 2 kOe for **1** and **2** are displayed in Fig. 2(a and b). At room temperature, the $\chi_M T$ values for **1** and **2** are 1.93 and 1.99 cm^3 K mol^{-1}, respectively, which are slightly larger than the spin-only value of 1.75 cm^3 K mol^{-1} anticipated from magnetically diluted $Ni^{II}Fe^{III}_2$ unit [two low-spin Fe^{III} ($S_{Fe} = 1/2$) and one Ni^{II} spins ($S_{Ni} = 1$) assuming $g_{Fe} = g_{Ni} = 2$]. The larger room temperature values are probably owing to the underestimated *g* values for Fe and Ni, which are often larger than 2.0.[22] Upon a decrease of the temperature, the $\chi_M T$ values of **1** and **2** increase slightly until reaching a maximum value of 2.09 cm^3 K mol^{-1} at 26 K for **1** and 2.24 cm^3 K mol^{-1} at 20 K for **2**, respectively, revealing the occurrence of ferromagnetic Ni^{II}···Fe^{III} interactions. The $\chi_M T$ curves for **1** and **2** in high temperature region indicate the ferromagnetic Ni^{II}···Fe^{III} interactions should be weak and further confirm that the larger room temperature $\chi_M T$ values than expected are due to *g* values rather than the Ni···Fe ferromagnetic contributions. Upon further cooling, the $\chi_M T$ values abruptly decreases to 0.34 and 1.10 cm^3 K mol^{-1} at *ca.* 1.8 K for **1** and **2**, respectively. The downturn of $\chi_M T$ values at low temperature can be ascribed to the intermolecular antiferromagnetic interactions and/or zero-field splitting effect.[22,30] The χ_M *vs.* *T* curve of **2** show monotonous increase upon cooling while a peak appears for **1** at about 3.5 K, indicating that an antiferromagnetic ordering might occur in **1**.[31] Curie–Weiss fitting for **1** and **2** based on $\chi_M = C/(T - \theta)$ was carried out between 20 and 300 K, affording $C = 1.96$ cm^3 K mol^{-1}, $\theta = 2.00$ K for **1** and $C = 2.01$ cm^3 K mol^{-1}, $\theta = 2.90$ K for **2**, respectively. The positive Weiss constants also suggest that the intracluster ferromagnetic interactions take place between magnetic centers through cyanide bridges.

To evaluate quantitatively the coupling constants for **1** and **2**, the linear trinuclear model based on Kambe's method[32] considering both the intra- and intermolecular contributions has been used to fit the $\chi_M T$ data. Based on the Hamiltonian $\hat{H} = -2JS_{Ni}(S_{Fe1} + S_{Fe2})$ (J represents the intramolecular coupling constant of Ni···Fe interactions), the magnetic formulas deduced can be written as:

$$\chi = \frac{Ng^2{\mu_B}^2}{3kT} \times \frac{A}{B},\ \chi_M = \frac{\chi}{1 - [2zj'/(Ng^2{\mu_B}^2)]\chi}$$

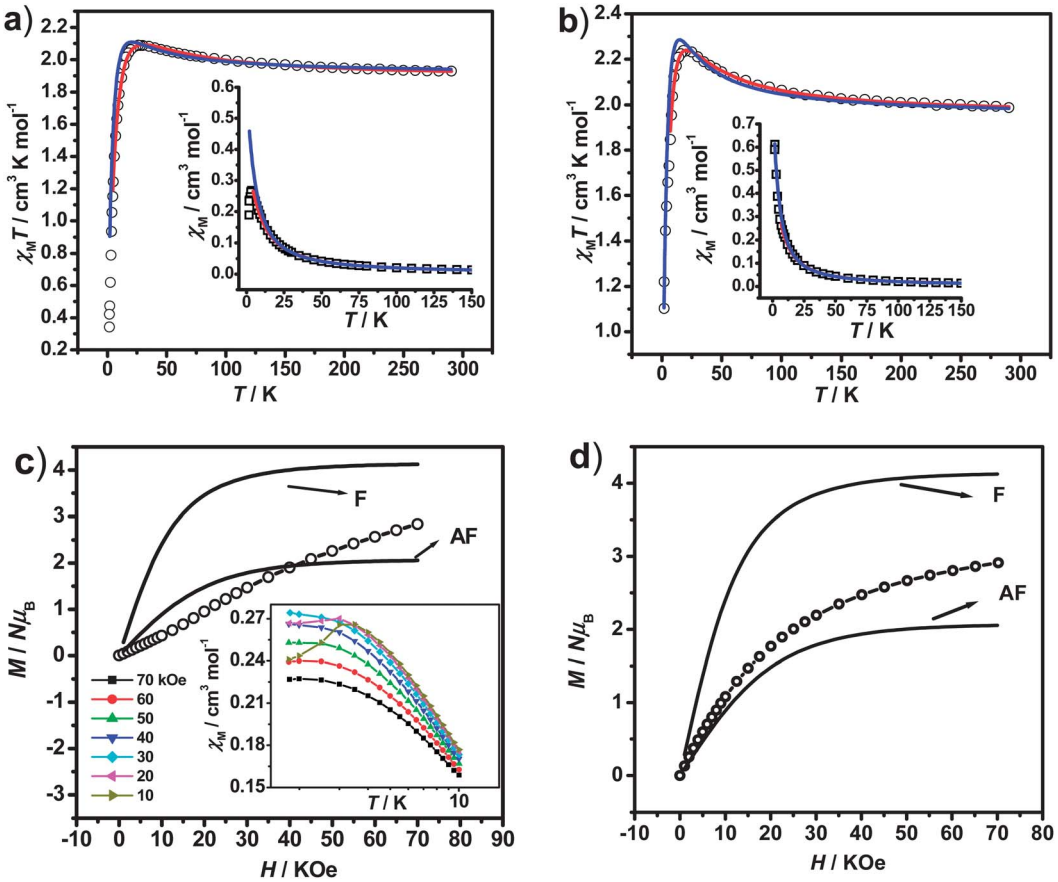

Fig. 2 Temperature dependence of $\chi_M T$ and χ_M (inset) for **1** (a) and **2** (b) measured at 2 kOe (the red and blue solid lines represent the best fits to the models described in the text); field dependence of the magnetization for **1** (c) and **2** (d) at 1.8 K (the curves marked with F, AF represent the theoretical Brillouin curves of ferro- and antiferromagnetic states of $NiFe_2$ unit; the inset shows the corresponding field-cooled magnetization for **1** in different applied fields).

$$A = 6 + 6e^{-2x} + 30e^{2x};\ B = 3 + e^{-4x} + 3e^{-2x} + 5e^{2x}$$

where $x = J/kT$, the N, g, k, T and μ_B have the common meanings, zj' represents the intermolecular interactions. The fitting curves [red solid line in Fig. 2(a and b)] for **1** (4.5–290 K) and **2** (7–290 K) match well with the experimental data, giving: $J = 7.09$ cm^{-1}, $g = 2.07$, $zj' = -1.33$ cm^{-1}, $R = 1.1 \times 10^{-4}$ for **1** and $J = 5.88$ cm^{-1}, $g = 2.11$, $zj' = -0.90$ cm^{-1}, $R = 1.0 \times 10^{-4}$ for **2**, respectively. Though the parameters can be used to reproduce the susceptibilities of **1** and **2**, the large zj' values seem to be unusual considering the crystal packing structures. Obviously, the zj' values were overestimated because the magnetic anisotropy brought by the Ni^{2+} ions can also contribute to the downturn of the $\chi_M T$ values. The J values should also be overestimated because of the large zj' values. The low temperature magnetic behaviors (1.8–60 K) are complicated because of the mixture contribution of intra-/intermolecular interactions and the magnetic anisotropy parameter, D_{Ni}. The Magpack program[33] can be used to evaluate the parameters. Based on the Hamiltonian $\hat{H} = -2JS_{Ni}(S_{Fe1} + S_{Fe2}) + D_{Ni}S_{z,Ni}^2$ and also taking into account the intermolecular interactions zj', the experimental data was simulated from 1.8–290 K. The best simulation shown in blue line in Fig. 2(a and b) corresponds to $J = 4.5$ cm^{-1}, $g = 2.09$, $|D_{Ni}| = 5.0$ cm^{-1}, $zj' = -0.5$ cm^{-1} for **1** and $J = 4.6$ cm^{-1}, $g = 2.11$, $|D_{Ni}| = 4.0$ cm^{-1}, $zj' = -0.2$ cm^{-1} for **2**, respectively. The D_{Ni} value is in the range of ones found in typical Ni complexes.[8b,22,34] The simulation parameters obtained quantitatively indicate that the single ion anisotropy D_{Ni} and weak intermolecular antiferromagnetic interactions zj' both contribute to the downturn of the $\chi_M T$ values, confirming that the zj' values extracted from the first model were overestimated. However, because the D and zj' parameters produce similar effects on low temperature magnetic behaviors and can not be estimated independently with a good accuracy, the parameters should also be taken with caution. The fitting results indicate that Ni···Fe coupling *via* cyanide bridges is ferromagnetic, with the coupling constants comparable to the analogous complexes reported.[7e,9g] It is worth noting that the intramolecular Ni^{II}···Fe^{III} interactions are always found to be ferromagnetic, which is easily understood considering the orbital orthogonality between low spin Fe^{III} ions (t_{2g}^5) and the Ni^{II} ions (e_g^2) bridged by cyanide groups. For comparison, some related cyano-bridged Fe^{III}–Ni^{II} complexes as well as structural and magnetic parameters are listed in Table 3. From the table, it can be found that larger Ni^{II}–N≡C angles often contribute to stronger magnetic exchange coupling. In fact, the larger Ni^{II}–N≡C angles in $Fe^{III}(Cr^{III})$–CN–Ni^{II} complexes can indeed

decrease the overlap of magnetic orbital and lead to stronger ferromagnetic interaction. Nevertheless, there are still many complexes showing inconsistency with the Ni^{II}–N≡C angle-dependant rule, suggesting some other structural factors such as metal–metal separations and/or torsion angles are also relevant to the exchange coupling strength.

To further study the low temperature magnetic behaviors, in particular for **1** which exhibits detectable magnetic ordering at very low temperature, field-dependent magnetization measurement (0–70 kOe at 1.8 K) was then performed. As shown in Fig. 2(c), the magnetization of **1** first increases linearly with the increase of external field, and then increases more rapidly until reaching about 2.84 $N\mu_B$ at 70 kOe, which is far from the saturation value of 4 $N\mu_B$ (calculated from $M_S = g(2S_{Fe} + S_{Ni})$ with $g = 2$) anticipated from ferromagnetic behaviors. For comparison, the theoretical Brillouin curves of ferro- and antiferromagnetic states of units of $Ni^{II}Fe_2{}^{III}$ were also plotted (Fig. 2(c)), which imply the presence of significant magnetic anisotropy in the system.[35] The magnetic behaviors of **1** revealed by *M*–*H* measurement are in accordance with the $\chi_M T$ result, and both of them indicate the presence of antiferromagnetic phase at very low temperature, which are overcome by the external field (critical field, $H_c = 20$ kOe) and lead to the sigmoid shape of the magnetization. This *M*–*H* curve for **1** suggests the metamagnetic-like behavior,[11,35b,36] which can be further evidenced by the measurement of susceptibility under different applied fields in the range of 1.8–10 K deduced by field-cooling magnetization (FCM) (Inset of Fig. 2(c)). Under low applied fields, the susceptibility curves show peaks at about 3.5 K, but the peaks become less prominent and invisible when the applied fields increase higher than 20 kOe, confirming the presence of metamagnetic transitions induced by the external fields. Associated with magnetic behaviors in high temperature regions, the antiferromagnetic ordering in **1** at very low temperature should derived from the intermolecular interactions mediated *via* π···π stacking or hydrogen bonds, as revealed by the structural analysis. However, no hysteresis loop can be detected for **1** in the temperature region explored, excluding the possibility of any metamagnet behaviors. Different from **1**, the magnetization of **2** (Fig. 2(d)) increases steadily with the increase of external field without sigmoid shape until reaching about 2.91 $N\mu_B$ at 70 kOe, which is also lower than the ferromagnetic saturated value (4 $N\mu_B$). The magnetization curve of **2** locates between the F and AF state of theoretical Brillouin curves, indicating the combined contributions from ferromagnetic exchanges and the single ion axial magnetic anisotropy.

Magnetic properties of 3 and 4. The temperature dependent of susceptibilities for **3** and **4** were also measured under 2 kOe, as plotted in Fig. 3(a and b). At room temperature, the $\chi_M T$ values for **3** and **4** are 1.34 and 1.35 $cm^3\ K\ mol^{-1}$, respectively, which are slightly larger than the spin-only value expected for the uncoupled $CuFe_2$ unit assuming $g_{Fe} = g_{Cu} = 2$, indicating the *g* values are higher than 2. Upon cooling, the $\chi_M T$ values of **3** and **4** both decrease gradually and then drop more rapidly until reaching 1.05 $cm^3\ K\ mol^{-1}$ for **3** and 0.41 $cm^3\ K\ mol^{-1}$ for **4** at 1.8 K, respectively. Curie–Weiss fitting for **3** and **4** was also performed between 20 and 300 K, affording $C = 1.35\ cm^3\ K\ mol^{-1}$, $\theta = -0.35$ K for **3** and $C = 1.37\ cm^3\ K\ mol^{-1}$, $\theta = -2.65$ K for **4**, respectively. The negative Weiss constant reveals that the intramolecular antiferromagnetic couplings are presented in **3** and **4**. The drop of the $\chi_M T$ curves at the low temperature are indicative of possible intermolecular antiferromagnetic interactions and/or zero-field splitting effect.[5a,37]

To evaluate the couplings constants, linear trinuclear model[9f] based on the Hamiltonian $\hat{H} = -2JS_{Cu}(S_{Fe1} + S_{Fe2})$ (J represents the intramolecular coupling constant of Cu···Fe interaction) has been used for fitting the data and the magnetic formulas can be expressed as (zj' represents the intermolecular interaction):

$$\chi = \frac{Ng^2\mu_B{}^2}{4kT} \times \frac{1 + 10e^{J/kT} + e^{-2J/kT}}{1 + 2e^{J/kT} + e^{-2J/kT}}$$

$$\chi_M = \frac{\chi}{1 - [2zj'/(Ng^2\mu_B{}^2)]\chi}$$

Table 3 Structural and magnetic parameters for selected cyano-bridged Fe^{III}–Ni^{II} complexes[a]

Complexes	Ni–N–C (degree)	*g*	J_{exp}/cm^{-1}	Ref.
$[(pzTp)Fe(CN)_3]_4[NiL]_4[OTf]_4 10DMF\cdot Et_2O$	177.4–179.1	2.20	6.6	9c
$\{[Ni(ntb)(MeOH)]_2[Fe(bbp)(CN)_3][ClO_4]_2\}\cdot 2MeOH$	176.5	2.22	8.61	22
$[Ni(L^*)][Fe(bpb)(CN)_2]_2\cdot 4H_2O$	173.4		7.7	26
$[(pzTp)Fe(CN)_2(\mu\text{-}CN)Ni(dmphen)_2]_2(ClO_4)_2\cdot 2CH_3OH$	170.3–171.6	2.39	6.2–8.4	9h
$[(pzTp)_2Fe_2(CN)_6Ni(bipy)_2]\cdot 2H_2O$	169.8	2.31	4.9	10
$[(Tp)_3(Tpm^{Me})_2Fe_3Ni_2(CN)_9]ClO_4\cdot 15H_2O$	168.4	2.27	4.84	7e
$\{[Ni(teta)][Fe(qcq)(CN)_3]_2\}\cdot 2DMF\cdot 2H_2O$	165.2	2.11	4.6	This work
$\{[Ni(en)_2][Fe(qcq)(CN)_3]_2\}\cdot 2H_2O$	161.5	2.09	4.5	This work
$[(dbphen)_2Fe_2(CN)_8Ni(dabhctd)]\cdot 2H_2O$	154.8	2.07	0.48	9f
$[(Tp)_2Fe(CN)_6Ni(en)_2]$	153.8	2.25	1.2	25
$[(pzTp)_2Fe_2(CN)_6Ni(L)]\cdot 1/2CH_3OH$	149.2–150.7	2.5	0.9	10

[a] Abbreviations used for the ligands: pzTp = tetra(pyrazol-1-yl)borate; L = 1,5,8,12-tetraazadodecane; bbp = bis(2-benzimidazolyl)pyridine dianion; L* = 3,10-bis(2-phenylethyl)-1,3,5,8,10,12-hexaazacyclotetradecane; bpb = 1,2-bis(pyridine-2-carboxamido)benzenate; dmphen = 2,9-dimethyl-1,10-phenanthroline; OTf: O_3SCF_3; Tp = hydrotris(pyrazol-1-yl)borate; Tpm^{Me} = tris(3,5-dimethyl-1-pyrazoyl)-methane; dbphen = 5,6-dibromo-1,10-phenanthroline; dabhctd = 1,8-di(amethylbenzyl)-1,3,6,8,10,13-hexaazacyclotetradecane.

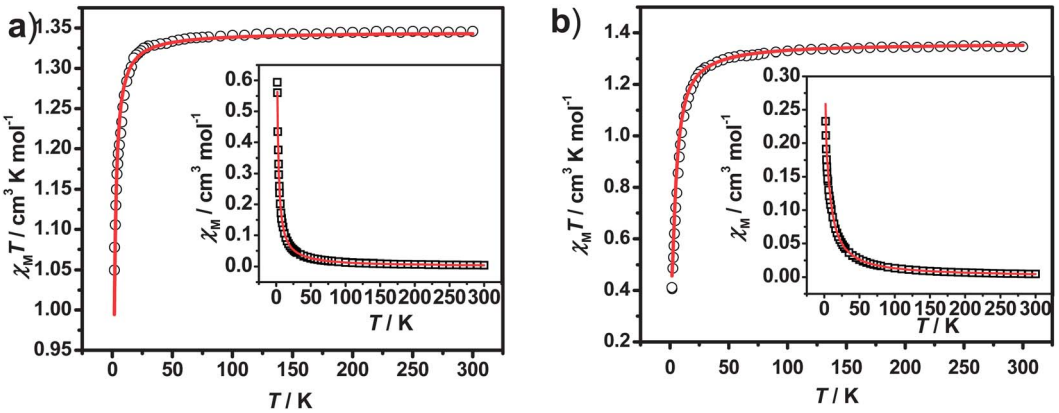

Fig. 3 Temperature dependence of $\chi_M T$ and χ_M (inset) for **3** (a) and **4** (b) measured at 2 kOe. (The red solid line represents the best fits to the model described in the text).

The best fits of the data of **3** and **4** in the whole temperature region gave: $J = -0.40$ cm^{-1}, $g = 2.18$, $zj' = -0.05$ cm^{-1}, $R = 2.2 \times 10^{-4}$ and $J = -2.56$ cm^{-1}, $g = 2.21$, $zj' = -0.1$ cm^{-1}, $R = 1.6 \times 10^{-4}$, respectively. The J value of **3** is comparable to that of the analogous $CuFe_2$ complexes,[29] but that for **4** seems to be slightly overestimated because of the pretty long Cu–N_{axial} bond length [2.559(2) Å]. Considering that cyanide nitrogen atoms in such systems usually occupy the axial positions of the elongated octahedral Cu surroundings, weak magnetic coupling should be expected. The fitting results further confirm the weak antiferromagnetic interactions presented in **3** and **4**. It is worth noting that most Fe^{III}–CN–Cu^{II} complexes display intramolecular ferromagnetic interactions,[9f,37,38] and antiferromagnetic examples are very rare.[29] The intramolecular ferromagnetic interactions in Fe^{III}–CN–Cu^{II} systems can be easily attributed to the strict orthogonality between the magnetic orbitals of low spin Fe^{III} ions (t_{2g}^5) and the Cu^{II} ions (e_g^3). However, to our knowledge, there are no systematically magneto–structural correlations investigations for antiferromagnetic magnetic exchanges of Fe^{III}–CN–Cu^{II} systems. So the antiferromagnetic couplings mechanism for Fe^{III}–CN–Cu^{II} systems is interesting and deserves further investigation.

Field-dependent magnetization measurement (0–70 kOe at 1.8 K) was also performed for **3** and **4** (Fig. 4) to verify the magnetic behaviors. As the external field increases, the magnetizations for **3** continuously increase until reaching 2.74 $N\mu_B$ at 70 kOe, which are larger than the theoretical values (1 $N\mu_B$) expected for the antiferromagnetic coupled $CuFe_2$ unit (calculated from $M_S = g(2S_{Fe}–S_{Cu})$ with $g = 2$). Suggesting the paramagnetic behaviors resulting from the decoupling effect of the weak antiparallely aligned spins by magnetic fields.[39] The decoupling effect can be readily reproduced by simulation of the M–H curves by Magpack (Fig. 4), where the weak antiferromagnetic coupled $CuFe_2$ unit can indeed show as large magnetization as uncoupled ones at high applied field. By comparing the experimental magnetizations with the simulated ones, the J value for **3** corresponds approximately to -0.5 cm^{-1}, which is in accord with the result provided by $\chi_M T$–T fittings. For **4**, the magnetization increases linearly until reaching 2.27 $N\mu_B$ at 70 kOe, which is consistent with the theoretical

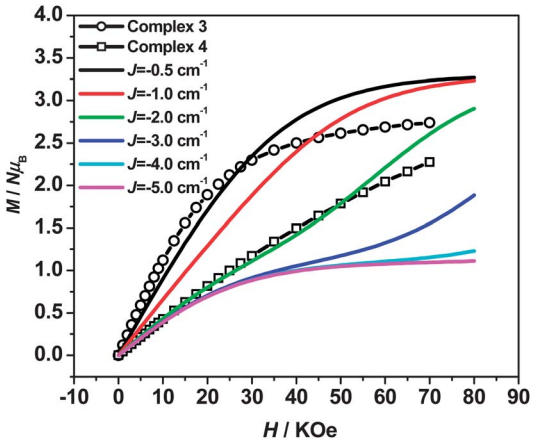

Fig. 4 Field-dependent magnetization for **3** and **4** (0–70 kOe at 1.8 K). The solid lines represent the simulated M–H curves for $CuFe_2$ unit assuming $J_{Fe-Cu} = 0.5–5.0$ cm^{-1} at 1.8 K.

simulated M–H curves corresponding to $J = -2.0$ cm^{-1}, indicating that the antiferromagnetic couplings are relatively stronger than **3**, but could also be decoupled by external field.

Conclusions

In this work, the *mer*-tricyanidoferrate building block, $[Fe^{III}(qcq)(CN)_3]^-$ has been used to successfully synthesize four new low dimensional cyano-bridged heterobimetallic complexes, which are shown as linear trinuclear $NiFe_2$ (**1**, **2**) and $CuFe_2$ (**3**, **4**) clusters. To our knowledge, these complexes are the first examples of Fe–CN–Ni(Cu) magnetic assembling using the latest designed *mer*-tricyanidoferrate building block, $[Fe^{III}(qcq)(CN)_3]^-$. The magnetic investigations reveal that intramolecular ferromagnetic Fe^{III}–CN–Ni^{II} interactions are presented in **1** and **2**, while the unusual intramolecular antiferromagnetic Fe^{III}–CN–Cu^{II} interactions were observed for **3** and **4**. The magnetic behaviors of **1** and **2** were well analyzed by considering the single ion anisotropy (D) of Ni^{II} ions. Interestingly, the unusual antiferromagnetic Fe^{III}–CN–Cu^{II} interactions were observed for **3** and **4**, and the weak magnetic couplings

could even be decoupled by strong applied field. The fully understanding of this unusual magnetic properties and clarifying the coupling mechanism need further investigation, related work is undergoing.

Acknowledgements

The authors are grateful for financial support from the National Natural Science Foundation of China (no. 51072071, 51272094 and 1601310042), Doctoral Innovation Program Foundation of China (no. 1721310119) and the Startup Foundation for Advanced Talents of Jiangsu University (no. 11JDG106).

Notes and references

1 (*a*) C. P. Berlinguette, D. Vaughn, C. Canada-Vilalta, J. R. Galan-Mascaros and K. R. Dunbar, *Angew. Chem., Int. Ed.*, 2003, **42**, 1523; (*b*) Y. Song, P. Zhang, X. M. Ren, X. F. Shen, Y. Z. Li and X. Z. You, *J. Am. Chem. Soc.*, 2005, **127**, 3708; (*c*) D. E. Freedman, D. M. Jenkins, A. T. Iavarone and J. R. Long, *J. Am. Chem. Soc.*, 2008, **130**, 2884; (*d*) J. J. Le Roy, M. Jeletic, S. I. Gorelsky, I. Korobkov, L. Ungur, L. F. Chibotaru and M. Murugesu, *J. Am. Chem. Soc.*, 2013, **135**, 3502.

2 (*a*) R. Clerac, H. Miyasaka, M. Yamashita and C. Coulon, *J. Am. Chem. Soc.*, 2002, **124**, 12837; (*b*) H. Miyasaka, A. Saitoh, M. Yamashita and R. Clerac, *Dalton Trans.*, 2008, 2422; (*c*) T. Liu, Y. J. Zhang, S. Kanegawa and O. Sato, *J. Am. Chem. Soc.*, 2010, **132**, 8250; (*d*) X. Feng, J. Liu, T. D. Harris, S. Hill and J. R. Long, *J. Am. Chem. Soc.*, 2012, **134**, 7521; (*e*) V. Tangoulis, M. Lalia-Kantouri, M. Gdaniec, C. Papadopoulos, V. Miletic and A. Czapik, *Inorg. Chem.*, 2013, **52**, 6559.

3 K. R. Dunbar, *Inorg. Chem.*, 2012, **51**, 12055.

4 (*a*) W. Wernsdorfer, N. Allaga-Alcalde, D. N. Hendrickson and G. Christou, *Nature*, 2002, **416**, 406; (*b*) H. L. Sun, Z. M. Wang and S. Gao, *Coord. Chem. Rev.*, 2010, **254**, 1081; (*c*) F. Troiani and M. Affronte, *Chem. Soc. Rev.*, 2011, **40**, 3119; (*d*) S. Sanvito, *Chem. Soc. Rev.*, 2011, **40**, 3336; (*e*) J. M. Clemente-Juan, E. Coronado and A. Gaita-Ariño, *Chem. Soc. Rev.*, 2012, **41**, 7464.

5 (*a*) M. J. Gunter, K. J. Berry and K. S. Murray, *J. Am. Chem. Soc.*, 1984, **106**, 4227; (*b*) K. V. Langenberg, S. R. Batten, K. J. Berry, D. C. R. Hockless, B. Moubaraki and K. S. Murray, *Inorg. Chem.*, 1997, **36**, 5006; (*c*) R. J. Parkera, L. Spiccia, B. Moubaraki, K. S. Murray, B. W. Skelton and A. H. White, *Inorg. Chim. Acta*, 2000, **300**, 922; (*d*) K. V. Langenberg, D. C. R. Hockless, B. Moubaraki and K. S. Murray, *Synth. Met.*, 2001, **122**, 573; (*e*) R. J. Parker, L. Spiccia, B. Moubaraki, K. S. Murray, D. C. Hockless, A. D. Rae and A. C. Willis, *Inorg. Chem.*, 2002, **41**, 2489; (*f*) D. E. Freedman, D. M. Jenkins and J. R. Long, *Chem. Commun.*, 2009, 4829; (*g*) P. V. Bernhardt, M. Martinez and C. Rodriguez, *Inorg. Chem.*, 2009, **48**, 4787; (*h*) D. Visinescu, L. M. Toma, J. Cano, O. Fabelo, C. Ruiz-Perez, A. Labrador, F. Lloret and M. Julve, *Dalton Trans.*, 2010, **39**, 5028; (*i*) X. Zhu, J. W. Zhao, B. L. Li, Y. Song, Y. M. Zhang and Y. Zhang, *Inorg. Chem.*, 2010, **49**, 1266; (*j*) S. Chorazy, K. Nakabayashi, K. Imoto, J. Mlynarski, B. Sieklucka and S. Ohkoshi, *J. Am. Chem. Soc.*, 2012, **134**, 16151; (*k*) D. P. Dong, Y. J. Zhang, H. Zheng, P. F. Zhuang, L. Zhao, Y. Xu, J. Hu, T. Liu and C. Y. Duan, *Dalton Trans.*, 2013, **42**, 7693.

6 (*a*) S. Ferlay, T. Mallah, R. Ouahes, P. Veillet and M. Verdaguer, *Nature*, 1995, **378**, 701; (*b*) O. Hatlevik, W. E. Buschmann, J. Zhang, J. L. Manson and J. S. Miller, *Adv. Mater.*, 1999, **11**, 914; (*c*) S. M. Holmes and G. S. Girolami, *J. Am. Chem. Soc.*, 1999, **121**, 5593.

7 (*a*) R. Lescouezec, J. Vaissermann, F. Lloret, M. Julve and M. Verdaguer, *Inorg. Chem.*, 2002, **41**, 5943; (*b*) J. Kim, S. Han, K. I. Pokhodnya, J. M. Migliori and J. S. Miller, *Inorg. Chem.*, 2005, **44**, 6983; (*c*) Z. H. Ni, H. Z. Kou, L. F. Zhang, C. Ge, A. L. Cui, R. J. Wang, Y. Li and O. Sato, *Angew. Chem., Int. Ed.*, 2005, **44**, 7742; (*d*) D. Li, S. Parkin, R. Clerac and S. M. Holmes, *Inorg. Chem.*, 2006, **45**, 7569; (*e*) Z. G. Gu, Q. F. Yang, W. Liu, Y. Song, Y. Z. Li, J. L. Zuo and X. Z. You, *Inorg. Chem.*, 2006, **45**, 8895; (*f*) M. Shatruk, A. Dragulescu-Andrasi, K. E. Chambers, S. A. Stoian, E. L. Bominaar, C. Achim and K. R. Dunbar, *J. Am. Chem. Soc.*, 2007, **129**, 6104; (*g*) F. Pan, Z. M. Wang and S. Gao, *Inorg. Chem.*, 2007, **46**, 10221; (*h*) C. G. Freiherr von Richthofen, A. Stammler, H. Bogge, M. W. DeGroot, J. R. Long and T. Glaser, *Inorg. Chem.*, 2009, **48**, 10165; (*i*) I. Boldog, F. J. Munoz-Lara, A. B. Gaspar, M. C. Munoz, M. Seredyuk and J. A. Real, *Inorg. Chem.*, 2009, **48**, 3710; (*j*) T. Liu, Y. J. Zhang, S. Kanegawa and O. Sato, *Angew. Chem., Int. Ed.*, 2010, **49**, 8645; (*k*) S. Nastase, C. Maxim, M. Andruh, J. Cano, C. Ruiz-Perez, J. Faus, F. Lloret and M. Julve, *Dalton Trans.*, 2011, **40**, 4898; (*l*) I. Y. Yoo, D. W. Ryu, J. H. Yoon, A. R. Sohn, K. S. Lim, B. K. Cho, E. K. Koh and C. S. Hong, *Dalton Trans.*, 2012, **41**, 1776; (*m*) M. X. Yao, Q. Zheng, X. M. Cai, Y. Z. Li, Y. Song and J. L. Zuo, *Inorg. Chem.*, 2012, **51**, 2140.

8 (*a*) R. Gheorghe, M. Kalisz, R. Clerac, C. Mathoniere, P. Herson, Y. Li, M. Seuleiman, R. Lescouezec, F. Lloret and M. Julve, *Inorg. Chem.*, 2010, **49**, 11045; (*b*) Y. H. Peng, Y. F. Meng, L. Hu, Q. Li, X. Y. Z. Li, J. L. Zuo and X. Z. You, *Inorg. Chem.*, 2010, **49**, 1905; (*c*) H. Y. Kwak, D. W. Ryu, J. W. Lee, J. H. Yoon, H. C. Kim, E. K. Koh, J. Krinsky and C. S. Hong, *Inorg. Chem.*, 2010, **49**, 4632; (*d*) M. Nihei, Y. Sekine, N. Suganami, K. Nakazawa, A. Nakao, H. Nakao, Y. Murakami and H. Oshio, *J. Am. Chem. Soc.*, 2011, **133**, 3592; (*e*) T. Liu, D. P. Dong, S. Kanegawa, S. Kang, O. Sato, Y. Shiota, K. Yoshizawa, S. Hayami, S. Wu, C. He and C. Y. Duan, *Angew. Chem., Int. Ed.*, 2012, **51**, 4367.

9 (*a*) R. Lescouezec, L. M. Toma, J. Vaissermann, M. Verdaguer, F. S. Delgado, C. Ruiz-Perez, F. Lloret and M. Julve, *Coord. Chem. Rev.*, 2005, **249**, 2691; (*b*) D. F. Li, S. Parkin, G. B. Wang, G. T. Yee, A. V. Prosvirin and S. M. Holmes, *Inorg. Chem.*, 2005, **44**, 4903; (*c*) D. Li, S. Parkin, G. Wang, G. T. Yee, R. Clerac, W. Wernsdorfer and S. M. Holmes, *J. Am. Chem. Soc.*, 2006, **128**, 4214; (*d*) L. Jiang, H. J. Choi, X. L. Feng, T. B. Lu and J. R. Long, *Inorg. Chem.*, 2007, **46**, 2181; (*e*) J. Z. Gu, L. Jiang, M. Y. Tan and T. B. Lu, *J. Mol.*

Struct., 2008, **890**, 24; (*f*) L. C. Kang, X. Chen, C. F. Wang, X. H. Zhou, J. L. Zuo and X. Z. You, *Inorg. Chim. Acta*, 2009, **362**, 5195; (*g*) Y. Z. Zhang, U. P. Malik, N. P. Rath, R. Clerac and S. M. Holmes, *Inorg. Chem.*, 2011, **50**, 10537; (*h*) E. Pardo, M. Verdaguer, P. Herson, H. Rousseliere, J. Cano, M. Julve, F. Lloret and R. Lescouezec, *Inorg. Chem.*, 2011, **50**, 6250.

10 D. Li, R. Clérac, S. Parkin, G. Wang, G. T. Yee and S. M. Holmes, *Inorg. Chem.*, 2006, **45**, 5251.

11 T. Senapati, C. Pichon, R. Ababei, C. Mathoniere and R. Clerac, *Inorg. Chem.*, 2012, **51**, 3796.

12 Z. H. Ni, H. Z. Kou, L. F. Zhang, W. W. Ni, Y. B. Jiang, A. L. Cui, J. Ribas and O. Sato, *Inorg. Chem.*, 2005, **44**, 9631.

13 J. I. Kim, H. S. Yoo, E. K. Koh, H. C. Kim and C. S. Hong, *Inorg. Chem.*, 2007, **46**, 8481.

14 J. I. Kim, H. S. Yoo, E. K. Koh and C. S. Hong, *Inorg. Chem.*, 2007, **46**, 10461.

15 J. L. Kim, H. Y. Kwak, J. H. Yoon, D. W. Ryu, I. Y. Yoo, N. Yang, B. K. Cho, J. G. Park, H. Lee and C. S. Hong, *Inorg. Chem.*, 2009, **48**, 2956.

16 O. Kahn, *Molecular Magnetism*, VCH, New York, 1993.

17 N. F. Curtis, *J. Chem. Soc.*, 1964, 2644.

18 M. P. Suh and S. G. Kang, *Inorg. Chem.*, 1988, **27**, 2544.

19 *Bruker, SMART. SAINT and XPREP: Area Detector Control and Data Integration and Reduction Software*, Bruker Analytical X-ray Instruments Inc.; Madison, Wisconsin, USA, 1995.

20 G. M. Sheldrick, *SADABS: Program for Empirical Absorption correction of Area Detector Data*, University of Göttingen, Göttingen, Germany, 1996.

21 G. M. Sheldrick, *SHELXL-97: Program for the Refinement of Crystal Structure*, University of Göttingen, Göttingen, Germany, 1997.

22 A. Panja, P. Guionneau, I. R. Jeon, S. M. Holmes, R. Clerac and C. Mathoniere, *Inorg. Chem.*, 2012, **51**, 12350.

23 H. Xiang, S. J. Wang, L. Jiang, X. L. Feng and T. B. Lu, *Eur. J. Inorg. Chem.*, 2009, 2074.

24 C. F. Wang, Z. G. Gu, X. M. Lu, J. L. Zuo and X. Z. You, *Inorg. Chem.*, 2008, **47**, 7957.

25 S. Wang, J. L. Zuo, H. C. Zhou, Y. Song and X. Z. You, *Inorg. Chim. Acta*, 2005, **358**, 2101.

26 Z. H. Ni, H. Z. Kou, Y. H. Zhao, L. Zheng, R. J. Wang, A. L. Cui and O. Sato, *Inorg. Chem.*, 2005, **44**, 2050.

27 S. Wang, J. L. Zuo, H. C. Zhou, Y. Song, S. Gao and X. Z. You, *Eur. J. Inorg. Chem.*, 2004, 3681.

28 R. Appelt and H. Vahrenkamp, *Z. Anorg. Allg. Chem.*, 2003, **629**, 133.

29 B. Zhang, Z. H. Ni, A. L. Cui and H. Z. Kou, *New J. Chem.*, 2006, **30**, 1327.

30 K. J. Cho, D. W. Ryu, H. Y. Kwak, J. W. Lee, W. R. Lee, K. S. Lim, E. K. Koh, Y. W. Kwon and C. S. Hong, *Chem. Commun.*, 2012, **48**, 7404.

31 (*a*) L. Toma, R. Lescouezec, J. Vaissermann, F. S. Delgado, C. Ruiz-Perez, R. Carrasco, J. Cano, F. Lloret and M. Julve, *Chem.–Eur. J.*, 2004, **10**, 6130; (*b*) X. P. Shen, Q. Zhang, H. B. Zhou, H. Zhou and A. H. Yuan, *New J. Chem.*, 2012, **36**, 1180.

32 K. Kambe, *J. Phys. Soc. Jpn.*, 1950, **5**, 48.

33 J. J. Borrts-Almenar, J. M. Clemente-Juan, E. Coronado and B. S. Tsukerblat, *J. Comput. Chem.*, 2001, **22**, 985.

34 G. Rogez, J. N. Rebilly, A. L. Barra, L. Sorace, G. Blondin, N. Kirchner, M. Duran, J. van Slageren, S. Parsons, L. Ricard, A. Marvilliers and T. Mallah, *Angew. Chem., Int. Ed.*, 2005, **44**, 1876.

35 (*a*) H. Miyasaka, H. Ieda, N. Matsumoto, K. Sugiura and M. Yama-shita, *Inorg. Chem.*, 2003, **42**, 3509; (*b*) H. B. Zhou, J. Wang, H. S. Wang, Y. L. Xu, X. J. Song, Y. Song and X. Z. You, *Inorg. Chem.*, 2011, **50**, 6868.

36 H. R. Wen, C. F. Wang, J. L. Zuo, Y. Song, X. R. Zeng and X. Z. You, *Inorg. Chem.*, 2006, **45**, 582.

37 M. Atanasov, C. Busche, P. Comba, F. El Hallak, B. Martin, G. Rajaraman, J. van Slageren and H. Wadepohl, *Inorg. Chem.*, 2008, **47**, 8112.

38 L. M. Toma, R. Lescouezec, J. Pasan, C. Ruiz-Perez, J. Vaissermann, J. Cano, R. Carrasco, W. Wernsdorfer, F. Lloret and M. Julve, *J. Am. Chem. Soc.*, 2006, **128**, 4842.

39 Q. Zhang, H. B. Zhou, X. P. Shen, H. Zhou and Y. Q. Yang, *New J. Chem.*, 2013, **37**, 941.

